

A Quantitative Investigation of Entrainment and Detrainment in Numerically Simulated
Convective Clouds. Part II: Simulations of Cumulonimbus Clouds.

1N-47
048 021

Charles Cohen
Institute for Global Change Research and Education*
Huntsville, Alabama

November, 1998

corresponding author address: Charles Cohen, Global Hydrology and Climate Center, 977
Explorer Blvd, Huntsville, AL 35806
E-mail: charlie.cohen@msfc.nasa.gov

* The Institute for Global Change Research and Education is jointly operated by the Universities Space Research Association and the University of Alabama in Huntsville.

A Quantitative Investigation of Entrainment and Detrainment in Numerically Simulated Convective Clouds. Part II: Simulations of Cumulonimbus Clouds

Charles Cohen
Institute for Global Change Research and Education*
Huntsville, Alabama

Abstract

Deep cumulonimbus clouds are simulated using a model that makes accurate diagnoses of entrainment and detrainment rates and of the properties of entrained and detrained air. Clouds generated by a variety of initial thermodynamic soundings are compared.

In the simulations, updraft entrainment rates are large near and above cloud base, through the entire depth of the conditionally unstable layer.

Stronger updrafts in a more unstable environment are better able to entrain relatively undisturbed environmental air, while weaker updrafts can entrain only air that has been modified by the clouds.

When the maximum buoyancy is large, the updraft includes parcels with a wide range of buoyancies, while weaker clouds are more horizontally uniform.

Strong downdrafts originate from levels at which updrafts detrain, and their mass flux depends on the mass flux of the updraft.

The magnitude of mixing between cloud and environment, not the entrainment rate, varies inversely with the cloud radius. How much of the mixed air is entrained depends on the buoyancy.

* The Institute for Global Change Research and Education is jointly operated by the Universities Space Research Association and the University of Alabama in Huntsville.

Abstract

Deep cumulonimbus clouds are simulated using a model that makes accurate diagnoses of entrainment and detrainment rates and of the properties of entrained and detrained air. Clouds generated by a variety of initial thermodynamic soundings are compared.

In the simulations, updraft entrainment rates are large near and above cloud base, through the entire depth of the conditionally unstable layer.

Stronger updrafts in a more unstable environment are better able to entrain relatively undisturbed environmental air, while weaker updrafts can entrain only air that has been modified by the clouds.

When the maximum buoyancy is large, the updraft includes parcels with a wide range of buoyancies, while weaker clouds are more horizontally uniform.

Strong downdrafts originate from levels at which updrafts detrain, and their mass flux depends on the mass flux of the updraft.

The magnitude of mixing between cloud and environment, not the entrainment rate, varies inversely with the cloud radius. How much of the mixed air is entrained depends on the buoyancy.

1. Introduction

It has always been difficult to obtain detailed knowledge of the dynamic and thermodynamic properties of clouds. Blyth (1993) discusses some specific problems connected with the use measuring devices within clouds. Limitations of radar prevented Grinnell *et al.* (1996) from observing motions near the base of the cloud updraft or outside the cloud edges, and induced them to calculate only the total vertical mass flux, instead of separate updraft and downdraft mass fluxes. Aircraft measurements may be biased, Jorgensen *et al.* (1985) explain, because the flight may not penetrate the center of a cloud updraft or downdraft. An additional limitation on gathering data within cumulonimbus clouds is the necessity for aircraft, in the interests of safety, to avoid the areas of strongest vertical velocity and greatest electrical activity.

Numerical cloud models have therefore been used to supplement observational data. One-dimensional models are easy to manipulate in order to design experiments, and their output is easy to interpret, but their validity is limited by the simplifying assumptions that are required to construct the models. Two- or three-dimensional primitive equation models, which are designed with relatively few simplifying assumptions, provide complete and physically consistent artificial data sets. Users of these models, however, may be overwhelmed with the massive quantities of data that the models can provide.

Part I (Cohen, 1998) of this study developed a method of diagnosing entrainment and detrainment rates and the properties of the entrained and detrained air in convective clouds simulated with a primitive equation model. We will now use this new technique to study deep cumulonimbus clouds.

2. Description of experiments

The Regional Atmospheric Modeling System (RAMS; Pielke *et al.*, 1992; Walko *et al.*, 1995) is used in this study, along with the tracers described in Part I, using an interval of 100 seconds between re-initializing the tracers.

All simulations are initialized with thermodynamic soundings that were constructed synthetically, based on the results of Betts (1986), Betts and Miller (1986), and Binder (1990), so that they could be systematically varied among the simulations.

Initial surface pressure and temperature are specified for each simulation. The soundings are conditionally unstable below the melting level. Above the melting level, the potential temperature increases with height up to a specified tropopause pressure, where the potential temperature has the value computed by lifting a parcel adiabatically from the surface. Temperature is constant with height above the specified tropopause pressure.

The moisture sounding is computed by prescribing the saturation level departures, P_D , P_m , and P_t , at the surface, the 0°C level, and the tropopause, respectively. The saturation level departure, following Betts (1982), is the difference in pressure between a parcel and its lifting condensation level (LCL). Given the surface pressure and temperature and P_D , the surface mixing ratio is computed. Potential temperature is constant up to the condensation level of a parcel lifted from the surface. To produce a planetary boundary layer that is partially mixed, the water vapor mixing ratio between the surface and the LCL is computed as 75% of the surface mixing ratio plus 25% of the mixing ratio that would result from using a constant saturation departure.

The degree of conditional instability between the LCL and the melting level is specified by the parameter, α , which is used to compute the vertical gradient of potential temperature as follows;

$$\frac{\partial \theta}{\partial p} = (1 - 0.1\alpha) \left(\frac{\partial \theta}{\partial p} \right)_{0_{ES}} \quad (1)$$

where $(\partial \theta / \partial p)_{0_{ES}}$ is the vertical gradient of potential temperature of the pseudo-adiabat through a surface parcel. Between the melting level and the tropopause, in order to produce an unstable midlatitude continental sounding, potential temperature is computed as 25% of what results from linearly interpolating potential temperature in pressure plus 75% of the result of linearly interpolating potential temperature in the logarithm of pressure. (For a maritime tropical sounding, linearly interpolating potential temperature in pressure may be more appropriate.) Water vapor mixing ratio between the LCL and the tropopause is then computed by linearly interpolating the saturation departure between P_b and P_m up to the melting level, and then interpolating between P_m and P_t above the melting level.

In all the simulations examined here, cloud updrafts are defined by $w > 0.5 \text{ m s}^{-1}$ and $q_c + q_i > 0.01 \text{ g kg}^{-1}$, where q_c and q_i are the mixing ratios of cloud water and pristine ice crystals, while cloud downdrafts are defined by $w < 0.5 \text{ m s}^{-1}$ and total condensate $> 0.01 \text{ g kg}^{-1}$. The first experiment is identical to the one described in Part I.

All initial soundings use a surface pressure of 1000 mb and a surface temperature of 304 K. Other quantities used to compute the initial soundings are listed in Table 1. A value of 3.0, appropriate for midlatitude continental convection, is assigned to the parameter, α , for the initial soundings in the first five experiments. Exps. 2 and 3 (Fig. 1b) use initial soundings that are drier and more moist, respectively, above the PBL. More stable soundings, that will produce weaker and shallower convection, are constructed for exps. 4 and 5 (Fig. 1c) by raising the LCL of surface air (*i.e.* by increasing the saturation level departures, P_b) in 50 mb increments while the tropopause is lowered in 50 mb increments.

Exp. 6 is initialized with a sounding that has nearly the same Convective Available Potential Energy (CAPE) as the sounding used to initialize the first experiment, but has a more stable lower troposphere (*i.e.* a smaller α) and a higher tropopause. These two soundings are shown in Fig. 1a.

3. Results

a. sensitivity to variations in the humidity of the initial sounding

The initial soundings (Table 1 and Fig. 1) of exps. 1, 2, and 3 are identical below 1 km, but the environment of exp. 2 is drier above the PBL than that of exp. 1, with a θ_e as much as 4.9 K lower in the middle troposphere, while exp. 3 uses a more moist environment above the PBL, with a θ_e as much as 3.6 K higher than in exp. 1. Greater humidity in the environment results in substantially more cloud mass flux (Fig. 2a).

For all three simulations, the updraft fractional entrainment rate (Fig. 3a) is largest near cloud base and decreases with height in the lower troposphere, but for a more moist environment, the entrainment rate decreases more slowly with height. This corresponds to the type of air that is being entrained. Fig. 4 compares the θ_e of the entrained air with the θ_e of an

equal mixture of updraft air and air from the undisturbed initial sounding. Starting just below 2 km, these two quantities are very similar, but, beginning at a higher level for a more moist initial sounding, the updraft entrains air with a higher θ_e than the equal mixture. At the higher levels, only the air that has been seriously modified by the clouds can be entrained into the updraft, and the fractional entrainment rate is therefore small (Fig. 3a); at lower levels, where air from the environment has a positive CAPE (Fig. 5a), more of the nearly undiluted environmental air can be entrained, and the fractional entrainment rate is large. The conditionally unstable air (Fig. 5a) and the larger entrainment rates (Fig. 3a) extend through a deeper layer above the surface for a more moist sounding.

To verify that the undisturbed initial sounding can be used to represent the environment of the clouds, θ_e was averaged, for the first 2.5 hours, when nearly all of the cloud mass flux occurred, over cloud-free grid points in an 80-km-wide area centered on the deep convection. When this environmental θ_e is substituted for the initial undisturbed θ_e , as shown in Fig. 4, the conclusions are unchanged.

For the more moist initial sounding (exp. 3) the deeper conditionally unstable layer enables the updraft mass flux to increase with height up to about 5 km (Fig. 2a). The updraft mass flux increases somewhat more rapidly with height in exp. 1 than in exp. 2 from cloud base up to 2 km, and also between 4 km and 6 km. Using the updraft mass flux and the fractional entrainment and detrainment rates, we can compute the entrained mass flux and the detrained mass flux. The results (Fig. 6) clearly show that the updraft continues both to grow and to mix with its environment through a deeper layer above cloud base with a more moist initial sounding.

It can be seen in Fig. 7 that, in the upper troposphere, the ratio of downdraft mass flux to updraft mass flux is larger for a drier environment, in which there is more evaporation or sublimation. Below 3 km, however, the clouds in the more moist environment have relatively more downdraft mass flux. (But the downdrafts are not stronger; the largest downward velocities in exps. 1, 2, and 3, are, respectively, -15 m s^{-1} , -16 m s^{-1} , and -14 m s^{-1} .) Whether the downdrafts are generated by the negative buoyancy that results from evaporation, melting, and condensate loading, or are dynamically forced, it is not surprising that a large downdraft mass flux is formed in the lower troposphere, where large amounts of cloudy air are detrained by the updraft. A stronger downdraft (Fig. 2a) extends through a deeper layer in the lower troposphere for the more moist environment, just as does the updraft detrainment. The ratio of downdraft mass flux to updraft mass flux is large when the updraft mass flux is increasing with height, because the downdraft at any level was generated by the updraft at a higher level.

Below 5 km, the vertical gradient of θ_e in the downdrafts is smaller for the more moist environment (Fig. 8). This is consistent with the downdraft entrainment rates (Fig. 3b), which peak at a greater height in the lower troposphere with a greater humidity. To predict the properties of the downdraft outflow, we must first determine the level of origin of the air in the low-level downdrafts. In the present simulations, this air is, on average, from a greater height, where θ_e is smaller, for the more moist environment. The more moist environment, therefore, generates more updraft mass flux, which produces, starting at a higher level, more low-level downdraft mass flux, bringing to the surface air with as low a θ_e as for a drier environment. Simpson et al. (1982) similarly concluded, based on their numerical simulations, that the strength of low-level cumulus downdrafts and their ability to bring mid-level low- θ_e air to the surface is proportional to the updraft strength. In contrast, Gilmore and Wicker (1998) found that

downdrafts in a drier environment in their simulations were stronger and brought lower θ_w air to the ground.

The present results do agree with those of Gilmore and Wicker (1998) in that downdraft CAPE, which measures the kinetic energy gained by an undilute parcel during descent, cannot be used to predict downdraft strength. Unless there is sufficient forcing by the updraft at a particular level, the potentially strong downdraft will not be realized.

b. sensitivity to the strength of the convection

When the soundings are changed, for exps. 4 and 5, in order to generate weaker convection with higher cloud bases and lower cloud tops, there is substantially less mass flux in both the updrafts and the downdrafts (Fig. 2b). With the most stable sounding, in exp. 5, the cloud downdrafts (*i.e.* according to the definition in Section 2) do not extend below 2 km, and only a very small amount of precipitation reaches the ground. The strongest upward velocities in exps. 1, 4, and 5 are, respectively, 32 m s⁻¹, 18 m s⁻¹, and 9 m s⁻¹.

A comparison of the maximum upward velocity to the velocity that would have resulted if all of the CAPE were converted to kinetic energy produces results similar to those of Zipser and LeMone (1980) and Jorgensen and LeMone (1989). Using the CAPE for air at the surface, the stronger updrafts achieve a greater fraction of the vertical velocity predicted from the CAPE. For exps. 1, 4, and 5, respectively, the strongest upward velocities are 38%, 28%, and 18% of the velocities 84 m s⁻¹, 65 m s⁻¹, and 49 m s⁻¹ predicted from the CAPE.

Because the mass fluxes shown in Fig. 2 are averages over space and time, and because the vertical velocities are different for the three simulations, the mass fluxes do not necessarily correspond to cloud radii. However, no cumulus parameterization is able to diagnose the cloud radius accurately; for those parameterizations which require a cloud radius, most arbitrarily specify one. One exception is that of Frank and Cohen (1987), who, assuming that increased mass flux in a grid column is accomplished by larger clouds rather than by more updrafts, specify an entrainment rate that decreases with an increasing mass flux. This is consistent with traditional 1D cloud models, which use an entrainment rate that is inversely proportional to the cloud radius. We might therefore expect exps. 1, 4, and 5 to have progressively larger entrainment rates.

In fact, the updraft entrainment rates (Fig. 9) are nearly the same between 3 km and 7.5 km. (Below 3 km, the large entrainment rates at different heights for the three simulations represent the air entering cloud base, while the cloud tops, where mass flux is small, produce large fractional entrainment rates at different levels between 8 km and 14 km.) Although the fractional entrainment rates are the same for the three simulations, the entrainment processes are not identical. For exps. 1, 4, and 5, respectively, between 3 km and 7.5 km in height, 36%, 24%, and 12% of the mass flux entrained into the updrafts is in mixtures containing more than 90% environmental air. The larger and stronger clouds are better able to entrain nearly undilute environmental air.

The conditional instability in the environment is different for the three simulations. When the initial soundings are made more stable in exps. 4 and 5, the CAPE (Fig. 5b) is significantly reduced for a parcel lifted from the surface, but the depth of the air with positive CAPE is changed only slightly. Consistent with this, the interval in which the θ_c of the entrained air is nearly the same as the θ_c of an equal mixture of updraft air and air from the undisturbed initial sounding extends slightly higher for the more unstable sounding (Fig. 10), but the differences are

not as great as for the soundings with variations in the humidity in the middle and upper troposphere (Fig. 4 and Section 3a). However, due to the higher cloud base, the height interval in which updrafts in exp. 5 entrain air characteristic of the equal mixture is a smaller than for exps. 1 and 4. Even within this height interval, θ_c of the entrained air for exp. 5 is slightly higher than that of the equal mixture, indicating that the weaker clouds are less able to entrain undilute environmental air, as shown in the previous paragraph.

It appears that, when entrainment is defined, as stated in section 2a of Part I, as including any clear air that becomes cloudy, then with a more unstable sounding, undilute, or nearly undilute environmental air above cloud base can more easily be entrained. Entrainment, then, as defined here, is not entirely a result of mixing between cloud and environment. Perhaps mixing, not entrainment, is inversely proportional to cloud radius.

To investigate this, we compute the amount of environmental air that has mixed with updraft air by adding the quantity $T_2 V$, where V is the volume of a grid box, at all grid points in which $0.01 < T_2/\rho < 0.99$ and $0.01 < T_5/\rho < 0.99$. Using the subset of these grid points which are in a cloud updraft gives the amount of environmental air that has mixed with updraft air and been entrained into the updraft. Adding $T_2 V$ over all grid points that are in a cloud updraft gives the amount of environmental air that has been entrained into the updraft, with or without mixing.

The results are shown in Fig. 11. (These quantities are assigned to the level at which the air was detected at the end of each interval; the procedure, described in section 2a of Part I, for assigning entrainment and detrainment rates to the correct levels was not used here.) The fraction of mixed air that was entrained is not significantly different for the three simulations. Averaged over the depth of the model, for exps. 1, 4, and 5, respectively, 32%, 32%, and 26% of the environmental air that mixed air with updraft air was entrained into the updraft. We do find substantial differences, however, when we compare the total amount of entrained air to the amount of mixed air. For exps. 1, 4, and 5, respectively, 28%, 20%, and 15% of the environmental air that was entrained into the updraft had not been mixed before being entrained. If we average over the height interval from 3 km to 7.5 km, where the entrainment rates are nearly the same (Fig. 9), the results are more dramatic; in this height interval, 34%, 19%, and 8% of the entrained air had not been mixed. Stated differently, between 3 km and 7.5 km, the ratio of environmental air that mixed with updraft air to environmental air that was entrained into the updraft is 2.2, 2.8, and 4.3 for exps. 1, 4, and 5. Averaged over the depth of the model, the same ratios are 2.2, 2.5, and 3.3. Therefore, for smaller clouds there is more mixing with the environment, but not necessarily more entrainment.

This supports the approach taken by Kain and Fritsch (1990), except that they do not account for undilute air joining the updraft above cloud base.

c. sensitivity to the buoyancy profile

The initial soundings in exps. 1 and 6 (Fig. 1a) are identical below 900 mb and have very similar values of CAPE, as shown in Fig. 5b. (For a parcel lifted from the surface, the CAPE is 3488 for exp. 1 and 3375 for exp. 6.) With a more stable lower troposphere and a higher tropopause, however, the buoyancy of an undilute parcel lifted from the surface in exp. 6 is higher in altitude than in exp. 1 (Fig. 12). Using 1.5 instead of 3.0 for the parameter, α , changes it from a value appropriate for a midlatitude continental sounding to one more characteristic of a tropical maritime sounding (*e.g.* Binder, 1990; his Table 3).

Despite the similar CAPE and the higher tropopause, the convection in exp. 6 is much weaker and slightly shorter than in exp. 1 (Fig. 2a), with a maximum upward velocity of 18 m s^{-1} , compared to 32 m s^{-1} for exp. 1.

To explain the weaker convection in exp. 6, we start by examining the properties of the entrained and detrained air, particularly between 4 km and 6 km, where the space- and time-averaged updraft mass flux is increasing with height in exp. 1 but decreasing with height in exp. 6 (Fig. 2a). This is near the 0°C level, where the two initial soundings differ the most (Fig. 1a). In exp. 1, the entrained air and detrained air have nearly the same θ_e at this level, and the updraft θ_e does not change much with height (Fig. 13a). In exp. 6, in contrast, the detrained air has a much higher θ_e than the entrained air, and the average θ_e of the updraft therefore decreases with height (Fig. 13b). With a relatively low buoyancy in the lower troposphere in exp. 6, only the most buoyant air can form a cloud, compared to exp. 3, in which air with a relatively large range of buoyancies can ascend in the updraft. Updraft properties in exp. 1 therefore have a larger variance (Fig. 14a). Between 4 km and 6 km, values of θ_e in the updraft in exp. 1 as much as 13 K higher than the mean, which is 340 K (Fig. 13a), are evidence of a nearly undilute core. The updraft in exp. 1 is detraining low- θ_e air from its periphery, while at the same level in exp. 6, the updraft is more uniform, and air representative of the updraft is being detrained.

Similarly, just above cloud base, where an undilute parcel is less buoyant in exp. 6 than in exp. 1 (Fig. 12), the updraft in exp. 6 is detraining air with a θ_e representative of the updraft, while only the low- θ_e air is being detrained from the updraft in exp. 1 (Fig. 13). Air with a wider range of θ_e is feeding the cloud updraft in exp. 1 (Fig. 14b), consistent with the greater low-level buoyancy of the most unstable air.

Between 4 km and 6 km, the initial sounding in exp. 6 is warmer than in exp. 1, with the same saturation level departure. Even though, at this level, there is no positive CAPE in the initial soundings (Fig. 5b), exp. 6 does have a higher θ_e than exp. 1. Consistent with this, the updraft in exp. 6 is entraining air with a θ_e close to that of an equal mixture of updraft air and air from the undisturbed initial sounding (Fig. 10), unlike exp. 1, in which the updraft is able to entrain only air which has been modified by the updraft to a greater extent.

If we compare the rate of entrainment to the rate of mixing with the environment for the updrafts in the two simulations, the greatest difference is that, in the lower troposphere, the ratio of entrained air to mixed air is much smaller in exp. 6 (Fig. 11). This is partly because less of the mixed air was entrained, and partly because less unmixed air joined the updraft.

By the time the updraft in exp. 6 reaches 9.5 km, where an undilute parcel would have a greater buoyancy than one in exp. 1, it has already been weakened by entrainment and detrainment to such an extent that it has a lower θ_e than the updraft in exp. 1 (Fig. 13). The buoyancy of an undilute parcel is therefore irrelevant at this height.

This comparison of exp. 1 and exp. 6 shows that, unlike Emanuel's (1991) model, whether or not cloud top is at the level of neutral buoyancy of an undilute parcel depends on the low-level buoyancy. In practice, the soundings used to initialize exps. 1 and 6 could be distinguished by following Blanchard's (1998) advice that CAPE be computed in a 3-km thick layer starting at the first level at which the density of a rising parcel would exceed that of its environment.

4. Discussion and conclusions

The fact that the mass flux in the updrafts is determined partly by the depth of the layer with positive CAPE, as shown in section 3a, has implications for the question, addressed by Lucas *et al.* (1994a, b, 1996) and Michaud (1996), of why midlatitude continental updraft cores have larger vertical velocities than maritime tropical updraft cores. Fig. 15 compares the CAPEs of air that originates at different levels in different types of soundings. The tropical soundings are from the Australian Monsoon Experiment (AMEX) stage 1 (Frank and McBride, 1989), and the GARP (Global Atmospheric Research Program) Atlantic Tropical Experiment (GATE) cloud clusters, stage 0 (Frank, 1978). Midlatitude soundings are taken from the Preliminary Regional Experiment for the Stormscale Operational and Research Meteorology Program (PRESTORM; Cuning, 1986). The Oklahoma City sounding was taken ahead of a squall line studied by Rutledge *et al.* (1988), Johnson and Hamilton (1988) and many others.

We see in Fig. 15 that the depth of the conditionally unstable air is much larger for the midlatitude continental soundings than for the maritime tropical soundings. In particular, the sounding from Woodward, Oklahoma, the same one used by Lucas *et al.* (1994a; their Fig. 9) has about the same maximum value of CAPE as the AMEX sounding, but it is obvious that, with sufficient horizontal convergence over a deep enough layer, the Woodward sounding can produce a cloud with more mass flux, and therefore a greater chance of including an undilute core. Furthermore, any entrainment that occurs in the first few kilometers above the ground would not decrease the buoyancy of the updraft as much as it would for the maritime tropical soundings. Of course, a 4.5 km-deep layer of air with positive CAPE is not typical, but the Oklahoma City sounding, with a maximum CAPE of over 4000, also has a deeper conditionally unstable layer than does either tropical sounding.

Lucas *et al.* (1994a) suggested that midlatitude continental clouds have larger diameters than do maritime tropical clouds because boundary layer eddies and hence the diameter of initial cumuliform clouds scale with the boundary layer depth, which is larger over the continents. The deeper conditionally unstable layer provides another possible explanation.

To simultaneously account for the degree of conditional instability in a sounding and the depth of the conditionally unstable layer, a vertically integrated CAPE (Mapes, 1993) or a generalized CAPE (Randall and Wang, 1992; Wang and Randall, 1994) may be useful.

Perry and Hobbs (1996) found that the methods developed by Bretherton and Smolarkiewicz (1989) and Taylor and Baker (1991) successfully predicted the levels at which air detrained from isolated cumulus clouds. We have seen here that the properties of the detrained air are also variable. The clouds simulated in this study, unlike those in traditional 1D cloud models, are not horizontally uniform. In particular, air detrained from clouds is not necessarily representative of the cloud at that level. With the large low-level buoyancy that is characteristic of mid-latitude continents, larger and stronger clouds, with nearly undilute cores, are generated, and only the low- θ_e air at the periphery is detrained. This influences the vertical gradient of the horizontally averaged θ_e in the cloud. Over a tropical ocean, with a more stable lower troposphere, only the air with the highest CAPE can ascend in the clouds, and the clouds are therefore narrower and more horizontally uniform, with more of the high- θ_e air mixing with the environment and detraining.

We summarize our conclusions as follows.

- Updraft entrainment rates are large near and above cloud base, through the entire depth of the conditionally unstable layer.
- Stronger updrafts in a more unstable environment are better able to entrain relatively undisturbed environmental air, while weaker updrafts can entrain only air that has been modified by the clouds.
- When the maximum buoyancy is large, the updraft includes parcels with a wide range of buoyancies, while weaker clouds are more horizontally uniform.
- Strong downdrafts originate from levels at which updrafts detrain, and their mass flux depends on the mass flux of the updraft.
- The magnitude of mixing between cloud and environment, not the entrainment rate, varies inversely with the cloud radius. How much of the mixed air is entrained depends on the buoyancy.

Acknowledgments

This work was done under NASA cooperative agreement #NCC8-142.

References

- Betts, A.K., 1982, Saturation point analysis of moist convective overturning. *J. Atmos. Sci.*, **39**, 1484-1505.
- , 1986: A new convective adjustment scheme. Part I: Observational and theoretical basis. *Quart. J. Roy. Meteor. Soc.*, **112**, 677-691.
- and M.J. Miller, 1986: A new convective adjustment scheme. Part II: Single column tests using GATE wave, BOMEX, ATEX and arctic air mass data sets. *Quart. J. Roy. Meteor. Soc.*, **112**, 693-709.
- Binder, P., 1990: On the parametric representation of the tropospheric thermodynamic structure for mid-latitude convective situations. *Quart. J. Roy. Meteor. Soc.*, **116**, 1349-1357.
- Blanchard, D.O., 1998: Assessing the vertical distribution of convective available potential energy. *Wea. Forecasting*, **13**, 870-877.
- Blyth, A.M., 1993: Entrainment in cumulus clouds. *J. Appl. Meteor.*, **32**, 626-641.
- Bretherton, C.S., and P.K. Smolarkiewicz, 1989: Gravity waves, compensating subsidence and detrainment around cumulus clouds. *J. Atmos. Sci.*, **46**, 740-759.
- Cohen, C., 1998: A quantitative investigation of entrainment and detrainment in numerically simulated convective clouds. Part I: Model development. *J. Atmos. Sci.*, submitted.
- Cunning, J.B., 1986: The Oklahoma-Kansas preliminary regional experiment for STORM-central. *Bull. Amer. Meteor. Soc.*, **67**, 1478-1486.
- Emanuel, K.A., 1991: A scheme for representing cumulus convection in large-scale models. *J. Atmos. Sci.*, **48**, 2313-2335.
- Frank, W.M., 1978: The life cycles of GATE convective systems. *J. Atmos. Sci.*, **35**, 1256-1264.
- and C. Cohen, 1987: Simulation of tropical convective systems. Part I: A cumulus parameterization. *J. Atmos. Sci.*, **44**, 3787-3799.
- and J.L. McBride, 1989: The vertical distribution of heating in AMEX and GATE cloud clusters. *J. Atmos. Sci.*, **46**, 3464-3478.
- Gilmore, M.S., and L.J. Wicker, 1998: The influence of midtropospheric dryness on supercell morphology and evolution. *Mon. Wea. Rev.*, **126**, 943-958.
- Grinnell, S.A., C.S. Bretherton, D.E. Stevens, and A.M. Fraser, 1996: Vertical mass flux calculations in Hawaiian trade cumulus clouds from dual-Doppler radar. *J. Atmos. Sci.*, **53**, 1870-1886.
- Johnson, R.H., and P.J. Hamilton, 1988: The relationship of surface pressure features to the precipitation and air flow structure of an intense midlatitude squall line. *Mon. Wea. Rev.*, **116**, 1444-1472.
- Jorgensen, D.P., E.J. Zipser, and M.A. LeMone, 1985: Vertical motions in intense hurricanes. *J. Atmos. Sci.*, **42**, 839-856.
- and M.A. LeMone, 1989: Vertical velocity characteristics of oceanic convection. *J. Atmos. Sci.*, **46**, 621-640.
- Kain, J.S., and J.M. Fritsch, 1990: A one-dimensional entraining/detraining plume model and its application in convective parameterization. *J. Atmos. Sci.*, **47**, 2784-2802.
- Lucas, C., E.J. Zipser, and M.A. LeMone, 1994a: Vertical velocity in oceanic convection off tropical Australia. *J. Atmos. Sci.*, **51**, 3183-3193.
- , -----, and -----, 1994b: Convective available potential energy in the environment of oceanic and continental clouds: Corrections and comments. *J. Atmos. Sci.*, **51**, 3829-3830.

- , -----, and -----, 1996: Reply. *J. Atmos. Sci.*, **53**, 1212-1214.
- Mapes, B.E., 1993: Gregarious tropical convection. *J. Atmos. Sci.*, **50**, 2026-2037.
- Mesinger, F., and A. Arakawa, 1976: Numerical methods used in atmospheric models. *GARP Publ. Ser. No. 17*, WMO-ICSU Joint Organizing Committee, 64 pp.
- Michaud, L.M., 1996: Comments on "Convective available potential energy in the environment of oceanic and continental clouds". *J. Atmos. Sci.*, **53**, 1209-1211
- Perry, K.D., and P.V. Hobbs, 1996: Influences of isolated cumulus clouds on the humidity of their surroundings. *J. Atmos. Sci.*, **53**, 159-174.
- Pielke, R.A., W.R. Cotton, R.L. Walko, C.J. Tremback, W.A. Lyons, L.D. Grasso, M.E. Nicholls, M.D. Moran, D.A. Wesley, T.J. Lee, and J.H. Copeland, 1992: A Comprehensive Meteorological Modeling System - RAMS. *Meteor. Atmos. Phys.*, **49**, 69-91.
- Randall, D.A., and J. Wang, 1992: The moist available energy of a conditionally unstable atmosphere. *J. Atmos. Sci.*, **49**, 240-255.
- Rutledge, S.A., R.A. Houze, Jr., M.I. Biggerstaff, and T. Matejka, 1988: The Oklahoma-Kansas mesoscale convective system of 10-11 June 1985: Precipitation structure and single-Doppler radar analysis. *Mon. Wea. Rev.*, **116**, 1409-1430.
- Simpson, J., G. Van Helvoirt, and M. McCumber, 1982: Three-dimensional simulations of cumulus congestus clouds on GATE day 261. *J. Atmos. Sci.*, **39**, 126-145.
- Taylor, G.R., and M.B. Baker, 1991: Entrainment and detrainment in cumulus clouds. *J. Atmos. Sci.*, **48**, 112-121.
- Walko, R.L., W.R. Cotton, M.P. Meyers, and J.Y. Harrington, 1995: New RAMS cloud microphysics parameterization. Part I: the single-moment scheme. *Atmos. Res.*, **38**, 29-62.
- Wang, J., and D.A. Randall, 1994: The moist available energy of a conditionally unstable atmosphere. Part II: Further analysis of GATE data. *J. Atmos. Sci.*, **51**, 703-710.
- Zipser, E.J., and M.A. LeMone, 1980: Cumulonimbus vertical velocity events in GATE. Part II: Synthesis and model core structure. *J. Atmos. Sci.*, **37**, 2458-2469.

Figure captions

- Fig. 1: Initial temperature and dewpoint soundings for (a) exp. 1 (solid) and exp. 6 (dashed), (b) exp. 2 (solid) and exp. 3 (dashed), and (c) exp. 4 (solid) and exp. 5 (dashed). The temperature soundings are identical for exps. 1, 2, and 3. The soundings shown by the solid lines are functions of pressure; height, shown on the right side, is computed for the soundings shown by the solid lines.
- Fig. 2: Horizontally averaged, time-averaged cloud mass flux for (a): exp. 1 (solid), exp. 2 (dashed), exp. 3 (dot-dash), and exp. 6 (dotted); and (b): exp. 1 (solid), exp. 4 (dashed), and exp. 5 (dotted). Updraft mass fluxes are shown by the positive curves; downdraft mass fluxes are shown by the negative curves
- Fig. 3: Fractional entrainment rates for the (a) updrafts and (b) downdrafts in exp. 1 (solid), exp. 2 (dashed), and exp. 3 (dotted).
- Fig. 4: Equivalent potential temperature of air entrained by the updraft (dashed) compared to an equal mixture of updraft air and air from the undisturbed initial sounding (solid) for exps. 1, 2, and 3. The dotted curves are for an equal mixture of updraft air and environmental air, which is computed as described in the text. For clarity, 4 K and 8 K have been added to the pairs of curves for exp. 1 and exp. 3, respectively.
- Fig. 5: CAPE computed from the initial soundings of (a) exp. 1 (solid), exp. 2 (dotted), and exp. 3 (dashed); and (b) exp. 1 (solid), exp. 4 (dotted), exp. 5 (dashed), and exp. 6 (dot-dash). The vertical axis shows the level of origin of the rising parcel.
- Fig. 6: Entrained (solid) and detrained (dashed) mass fluxes in the updrafts for (a) exp. 2, (b) exp. 1, and (c) exp. 3.
- Fig. 7: Ratio of downdraft mass flux to updraft mass flux for exp. 1 (solid), exp. 2 (dashed), and exp. 3 (dotted).
- Fig. 8: Average equivalent potential temperature for the downdrafts in exp. 1 (solid), exp. 2 (dashed), and exp. 3 (dotted).
- Fig. 9: Fractional entrainment rates for the updrafts in exp. 1 (solid), exp. 4 (dashed), and exp. 5 (dotted).
- Fig. 10: Equivalent potential temperature of air entrained by the updraft (dashed) compared to an equal mixture of updraft air and air from the undisturbed initial sounding (solid) for exps. 1, 4, 5, and 6. For clarity, 6 K has been added to the pair of curves for exp. 6.
- Fig. 11: Mass of environmental air that mixed with updraft air (dashed), mass of environmental air that mixed with updraft air and was entrained into the updraft (solid), and mass of environmental air that was entrained into the updraft, with or without mixing (dotted), for (a) exp. 1, (b) exp. 4, (c) exp. 5, and (d) exp. 6.
- Fig. 12: Virtual temperature of air parcel minus environmental value for pseudoadiabatic ascent from the surface, using the initial undisturbed soundings of exp. 1 (solid) and exp. 6 (dashed).
- Fig. 13: Equivalent potential temperature in (a) exp. 1 and (b) exp. 6: undisturbed initial sounding (solid), updraft (dashed), entrained by the updraft (dot-dash), and detrained by the updraft (dotted).
- Fig. 14: Probability density function of deviations of updraft θ_e from its mean value for updrafts at the same level, for exp. 1 (solid) and exp. 6 (dotted), for (a) the height interval from 3.9 km to 6.0 km, and (b) the height interval from the surface up to 3 km.

Fig. 15: CAPE computed from soundings observed at Woodward, Oklahoma, 0130 UTC 11 June 1985 (solid), and at Oklahoma City 2030 UTC 10 June 1985 (dot-dash), and for composites of cloud clusters observed during GATE (dotted) and AMEX (dashed). The vertical axis shows the level of origin of the rising parcel.

Table 1: Quantities used to compute initial soundings.

Exp.	P_b	P_m	P_t	P_{trop}	α
1	100	50	30	150	3
2	100	100	50	150	3
3	100	20	10	150	3
4	150	50	30	200	3
5	200	50	30	250	3
6	100	50	30	125	1.5

P_b , P_m , and P_t are the saturation level departures at the surface, the 0°C level, and the tropopause, respectively.

P_{trop} is the tropopause pressure.

α specifies the degree of conditional instability in the lower troposphere, using Eq. 1.

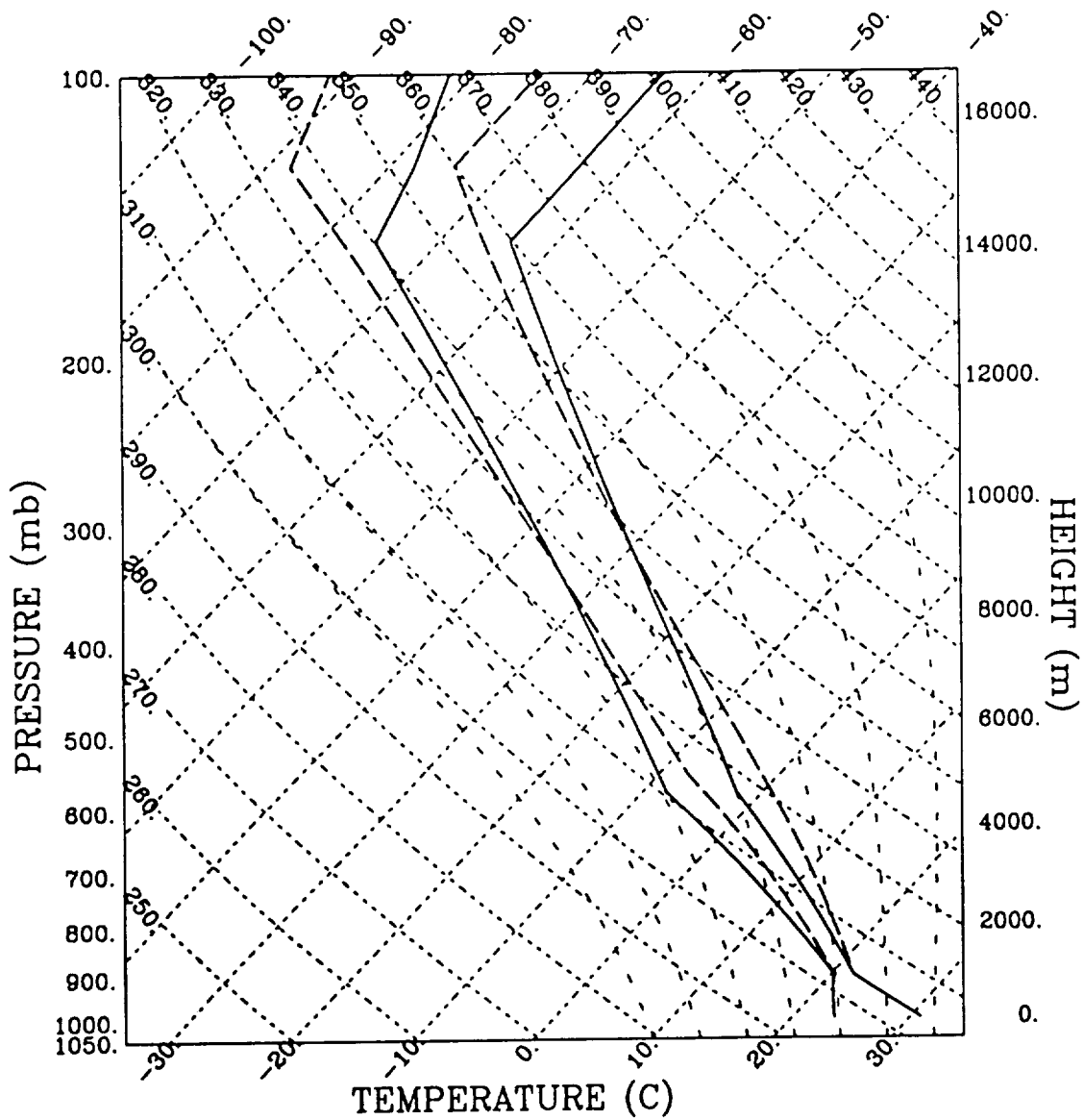


Fig. 1a: Initial temperature and dewpoint soundings for exp. 1 (solid) and exp. 6 (dashed). The soundings are functions of pressure; height, shown on the right side, is computed for the sounding shown by the solid lines.

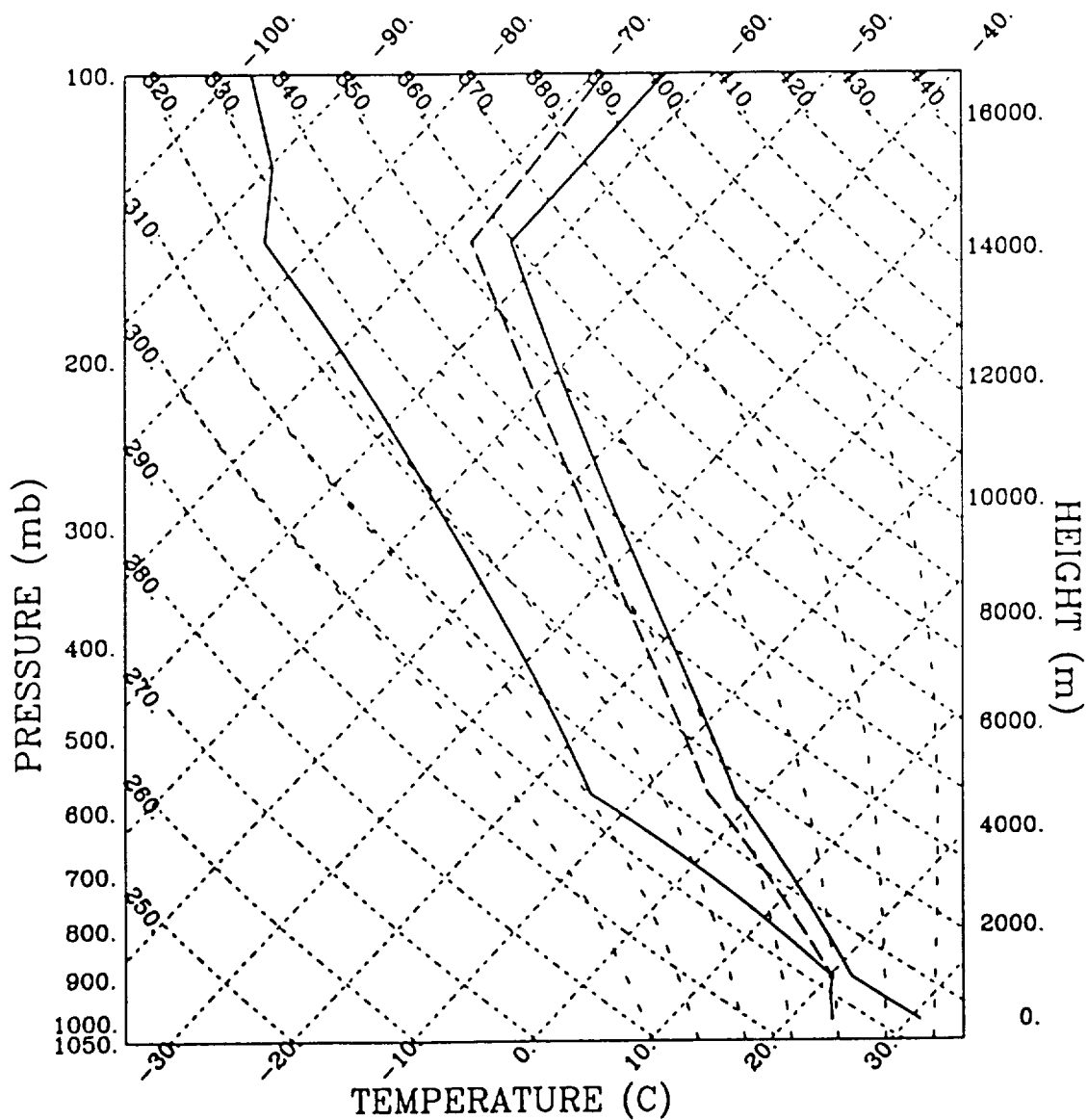


Fig. 1b: Initial temperature and dewpoint soundings for exp. 2 (solid) and exp. 3 (dashed). The temperature soundings are identical for exps. 1, 2, and 3. The soundings are functions of pressure; height, shown on the right side, is computed for the soundings shown by the solid lines.

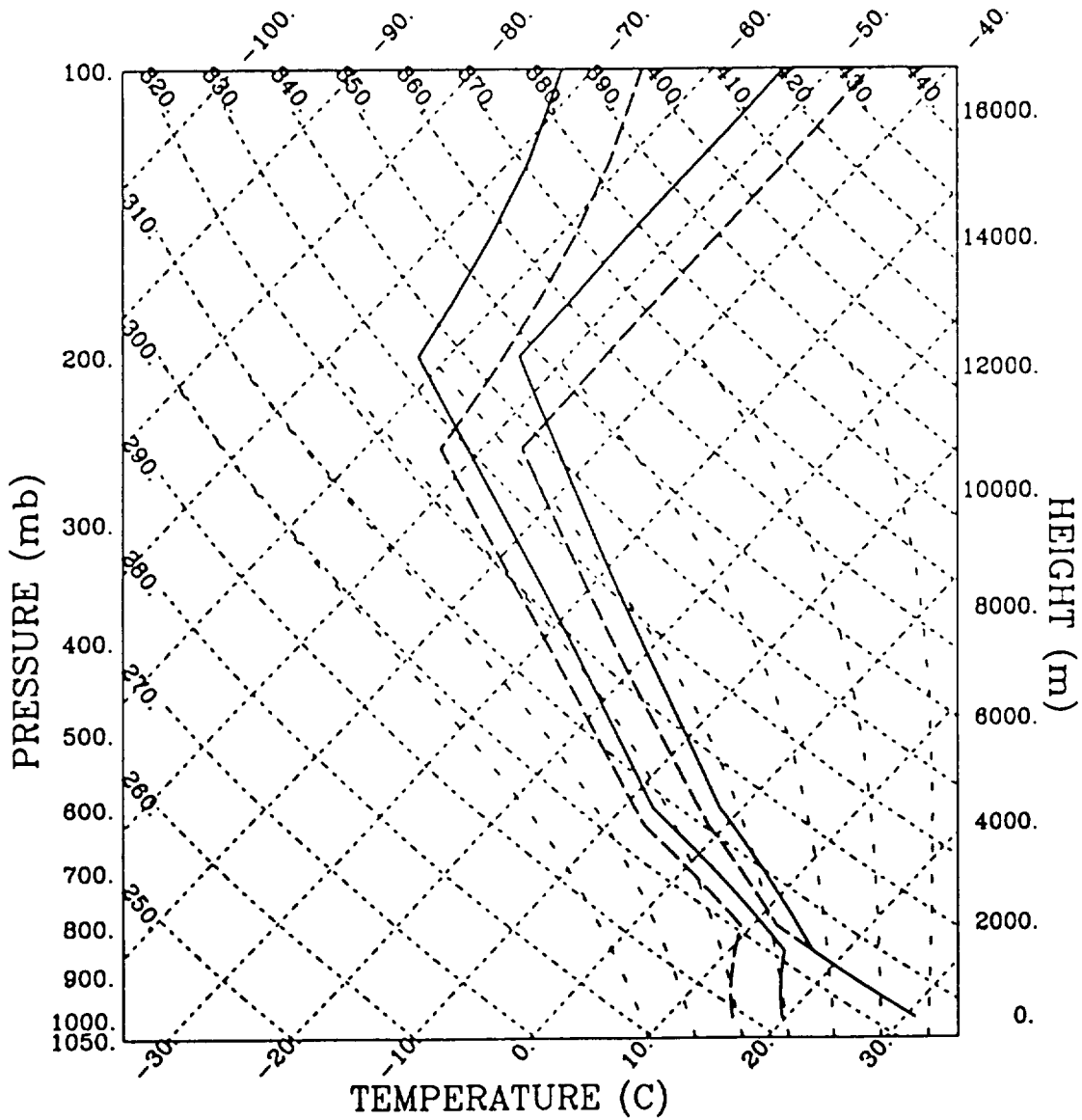


Fig. 1c: Initial temperature and dewpoint soundings for exp. 4 (solid) and exp. 5 (dashed). The soundings are functions of pressure; height, shown on the right side, is computed for the soundings shown by the solid lines.

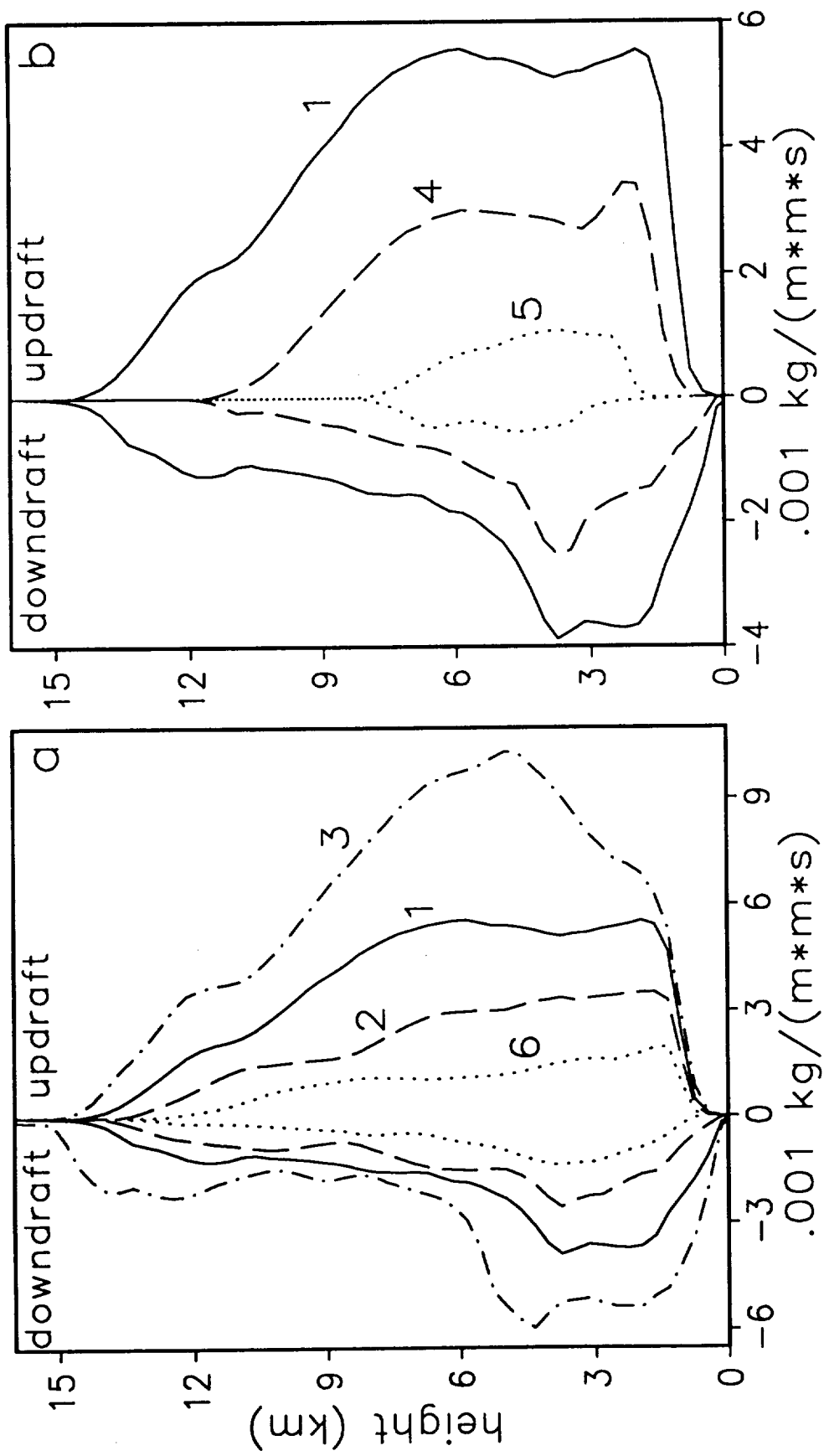


Fig. 2: Horizontally averaged, time-averaged cloud mass flux for (a) exp. 1 (solid), exp. 2 (dashed), exp. 3 (dot-dash), and exp. 6 (dotted); and (b) exp. 1 (solid), exp. 4 (dashed), and exp. 5 (dotted). Updraft mass fluxes are shown by the positive curves; downdraft mass fluxes are shown by the negative curves.

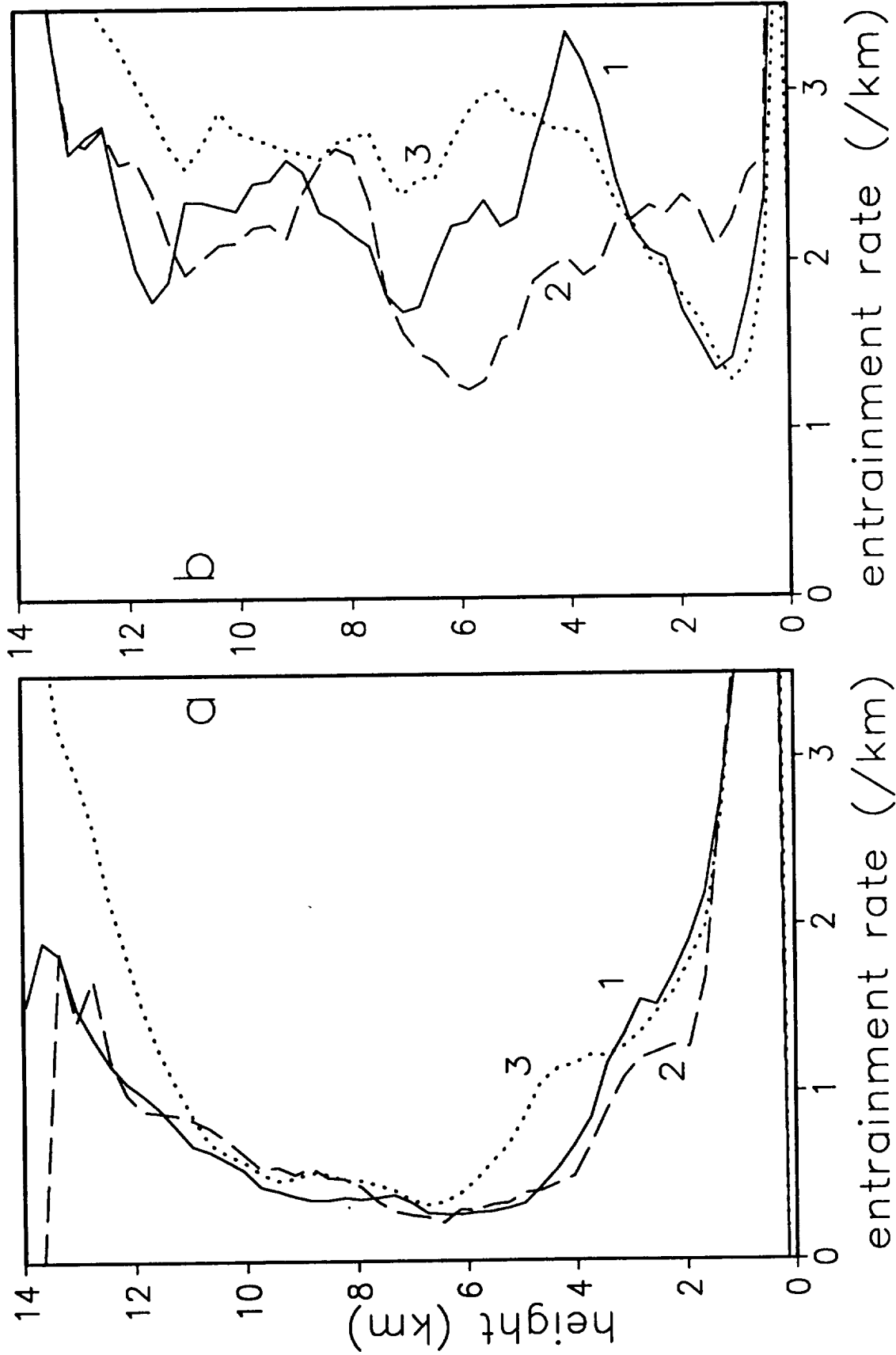


Fig. 3: Fractional entrainment rates for the (a) updrafts and (b) downdrafts in exp. 1 (solid), exp. 2 (dashed), and exp. 3 (dotted).

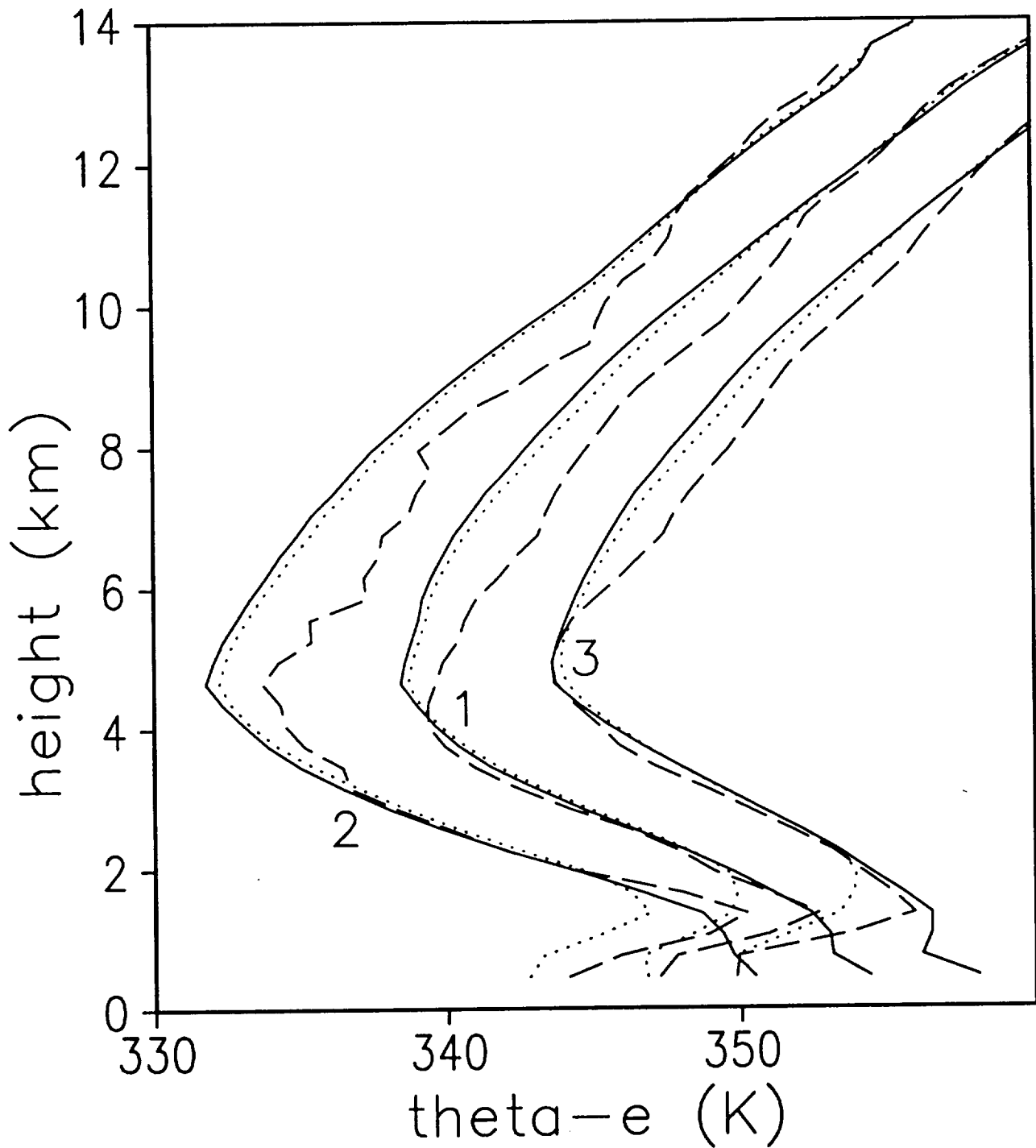


Fig. 4: Equivalent potential temperature of air entrained by the updraft (dashed) compared to an equal mixture of updraft air and air from the undisturbed initial sounding (solid) for exps. 1, 2, and 3. The dotted curves are for an equal mixture of updraft air and environmental air, which is computed as described in the text. For clarity, 4 K and 8 K have been added to the pairs of curves for exp. 1 and exp. 3, respectively.

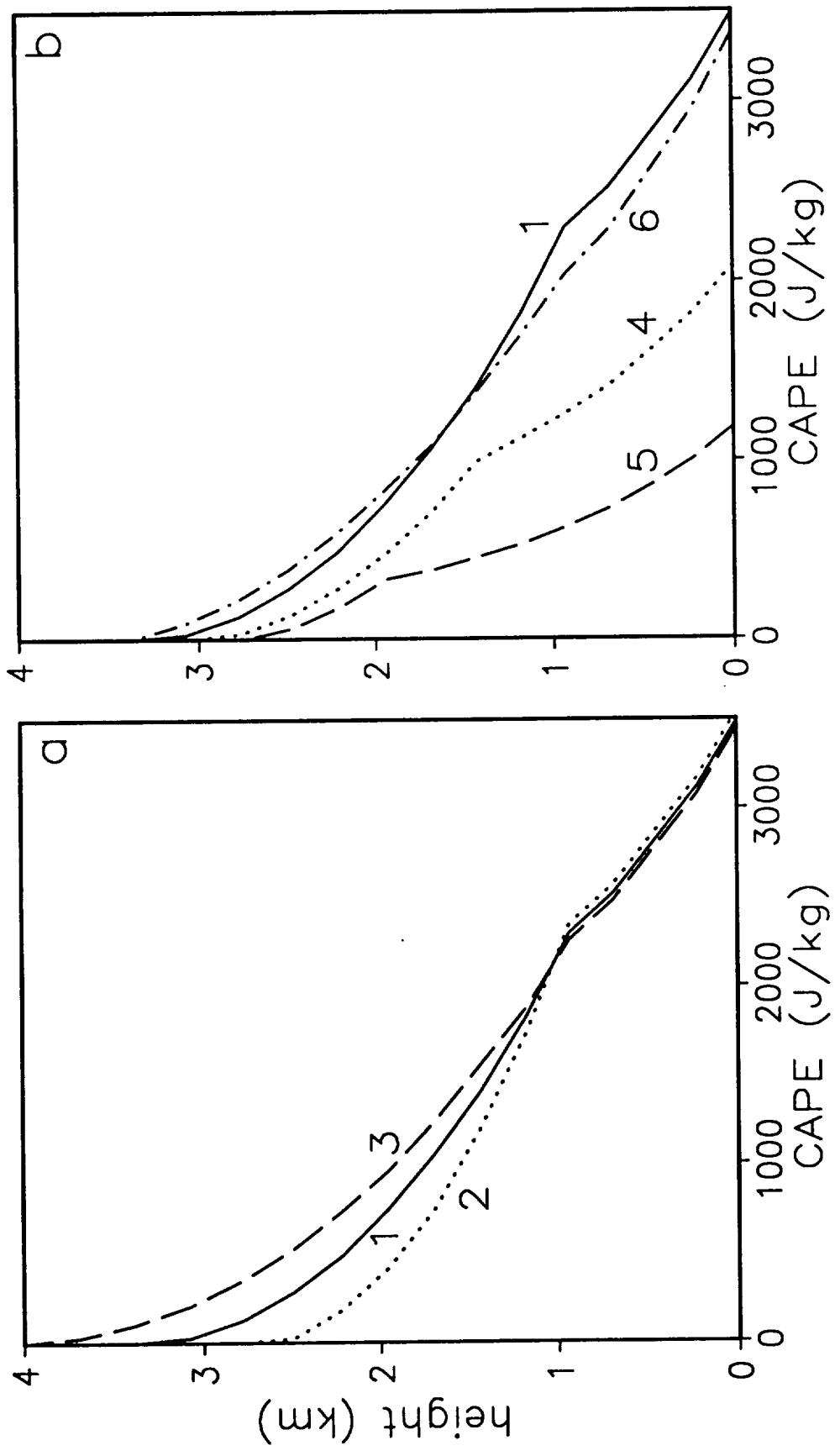


Fig. 5: CAPE computed from the initial soundings of (a) exp. 1 (solid), exp. 2 (dotted), and exp. 3 (dashed); and (b) exp. 1 (solid), exp. 4 (dotted), exp. 5 (dashed), and exp. 6 (dot-dash). The vertical axis shows the level of origin of the rising parcel.

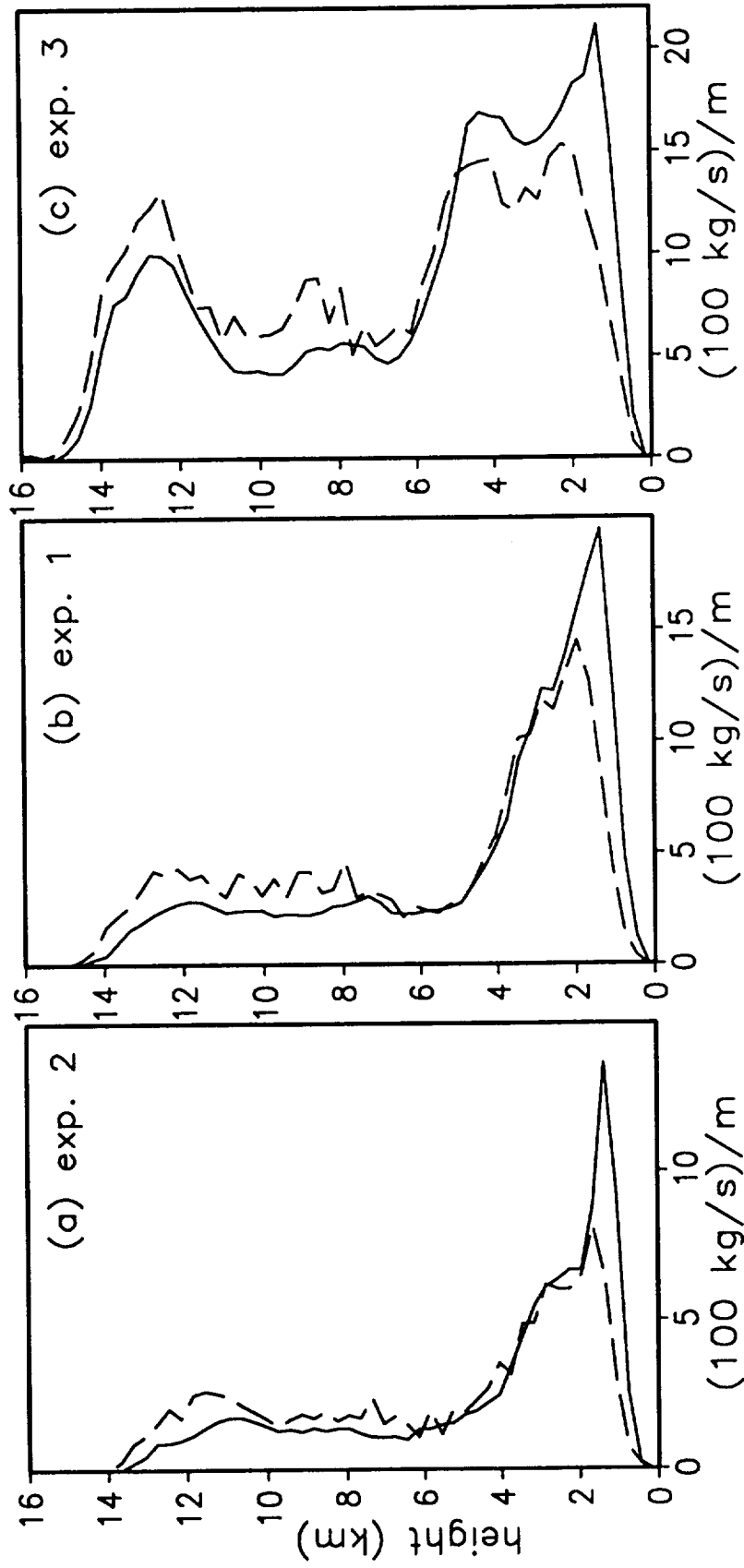


Fig. 6: Entrained (solid) and detrained (dashed) mass fluxes in the updrafts for (a) exp. 2, (b) exp. 1, and (c) exp. 3.

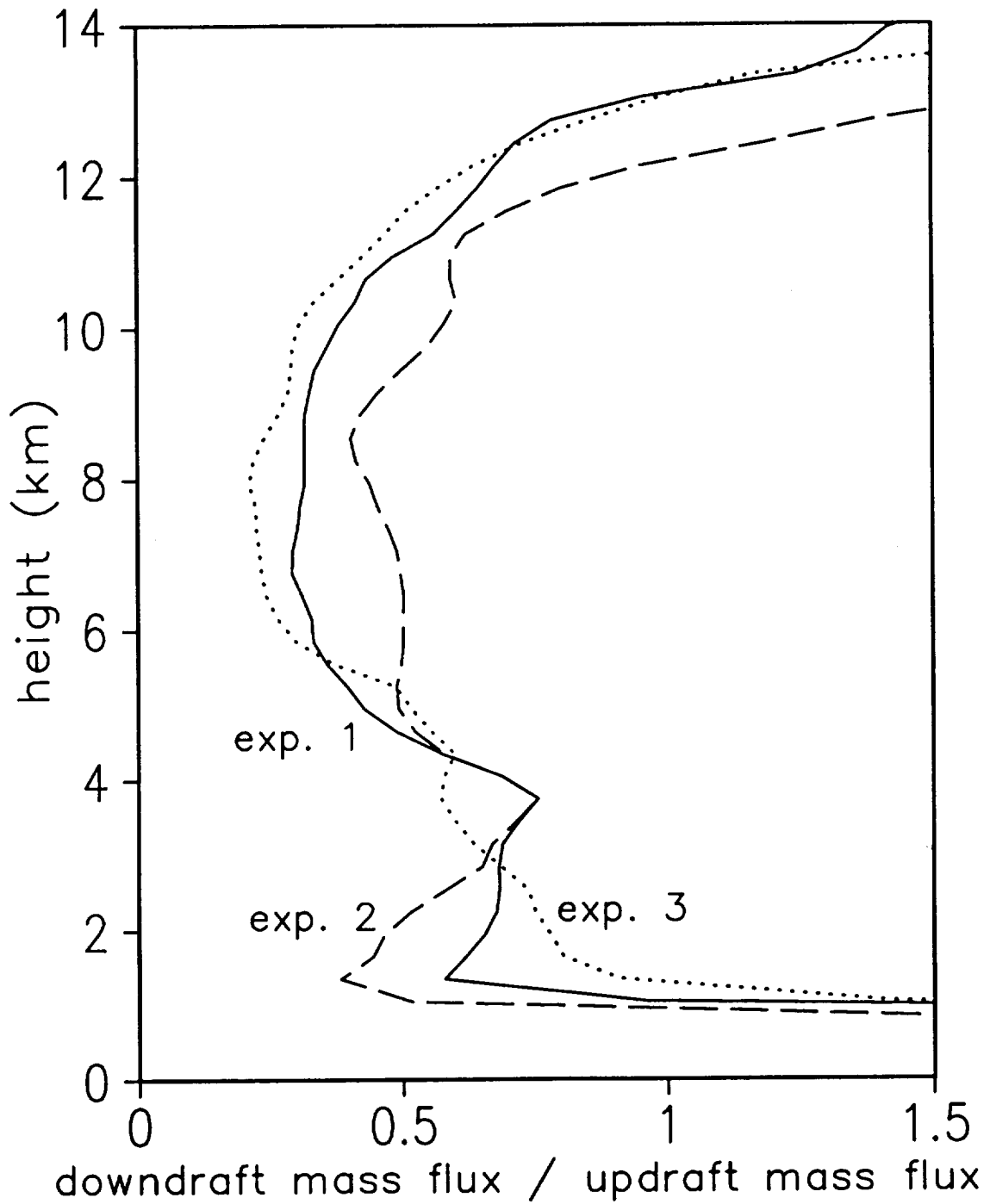


Fig. 7: Ratio of downdraft mass flux to updraft mass flux for exp. 1 (solid), exp. 2 (dashed), and exp. 3 (dotted).

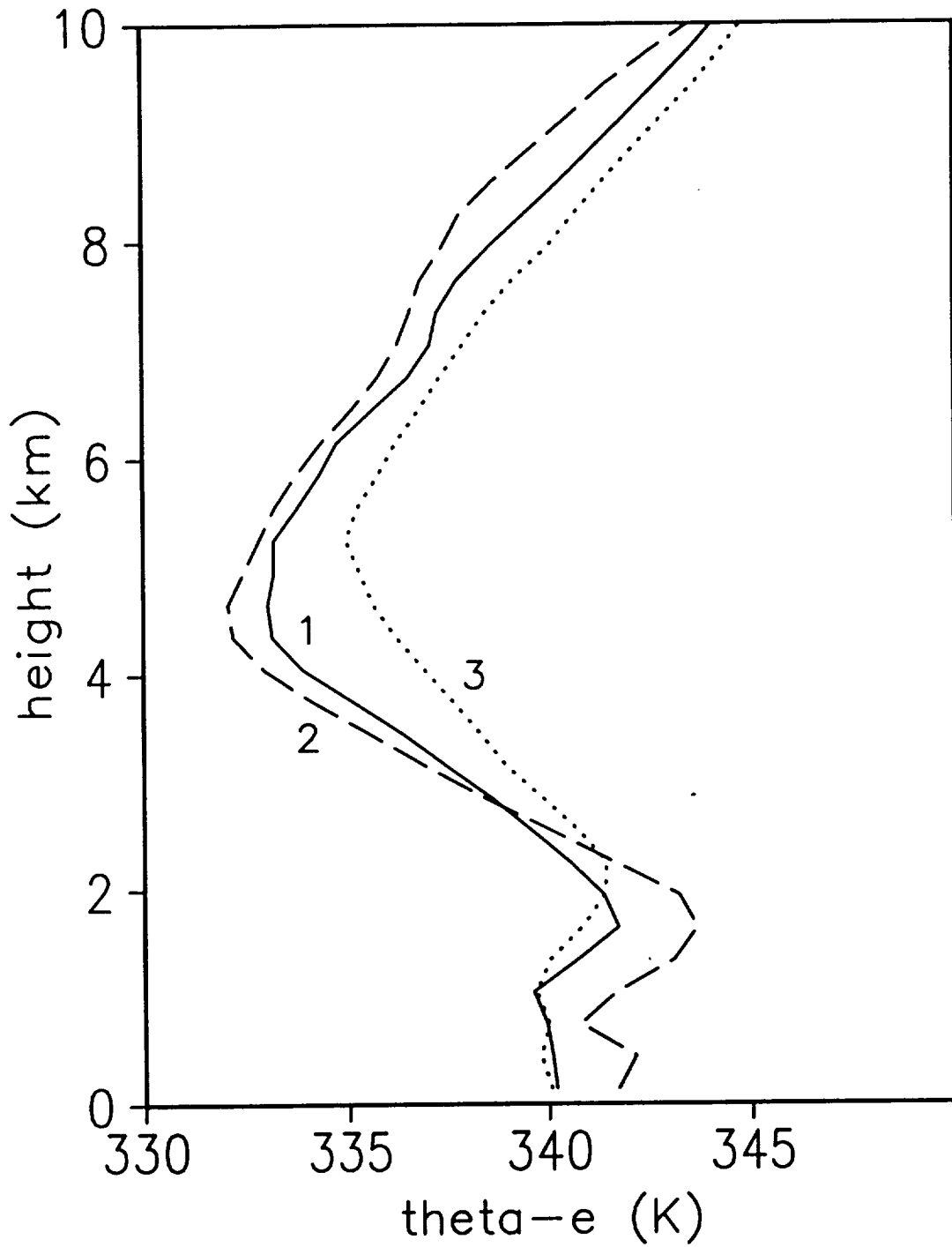


Fig. 8: Average equivalent potential temperature for the downdrafts in exp. 1 (solid), exp. 2 (dashed), and exp. 3 (dotted).

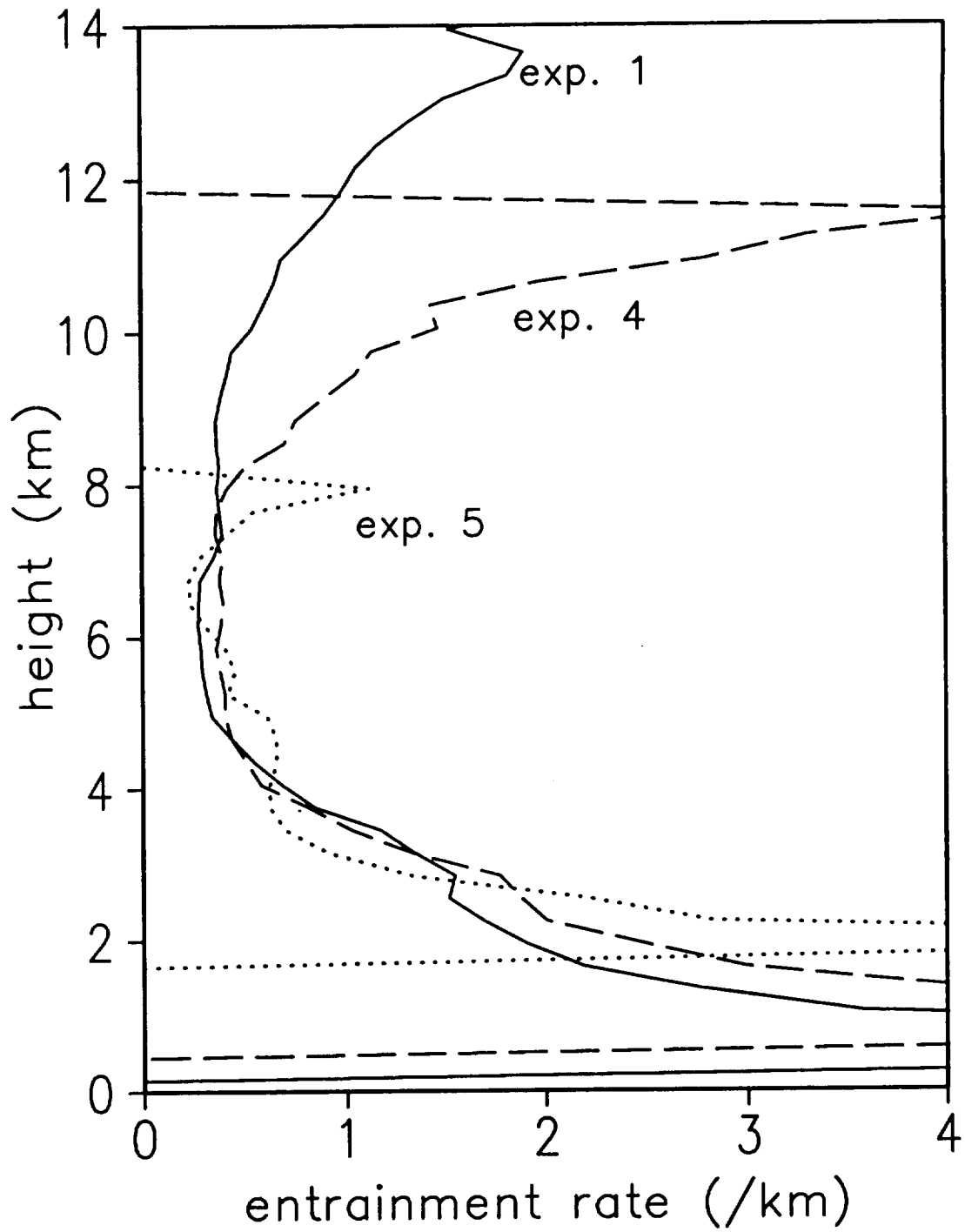


Fig. 9: Fractional entrainment rates for the updrafts in exp. 1 (solid), exp. 4 (dashed), and exp. 5 (dotted).

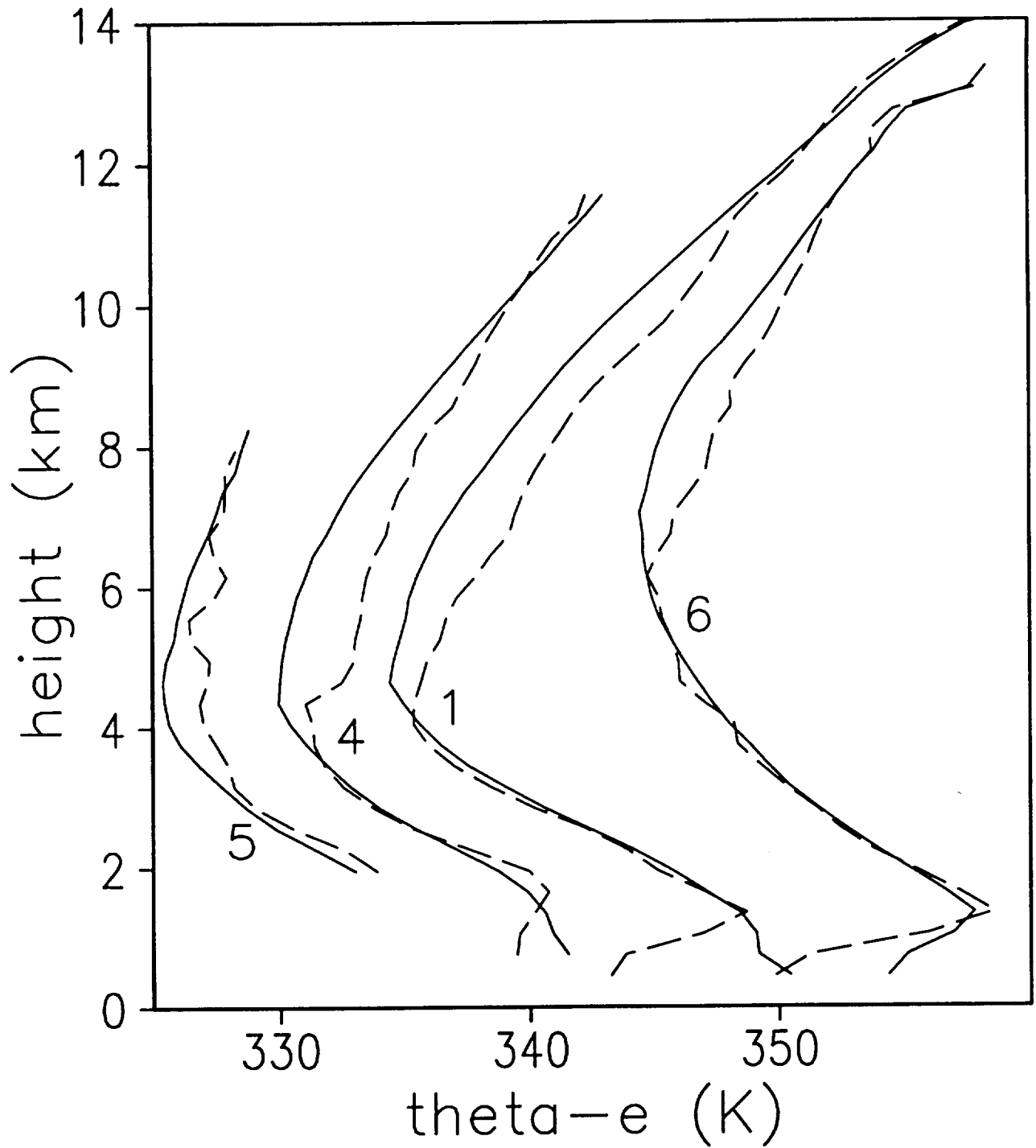


Fig. 10: Equivalent potential temperature of air entrained by the updraft (dashed) compared to an equal mixture of updraft air and air from the undisturbed initial sounding (solid) for expts. 1, 4, 5, and 6. For clarity, 6 K has been added to the pairs of curves for exp. 6.

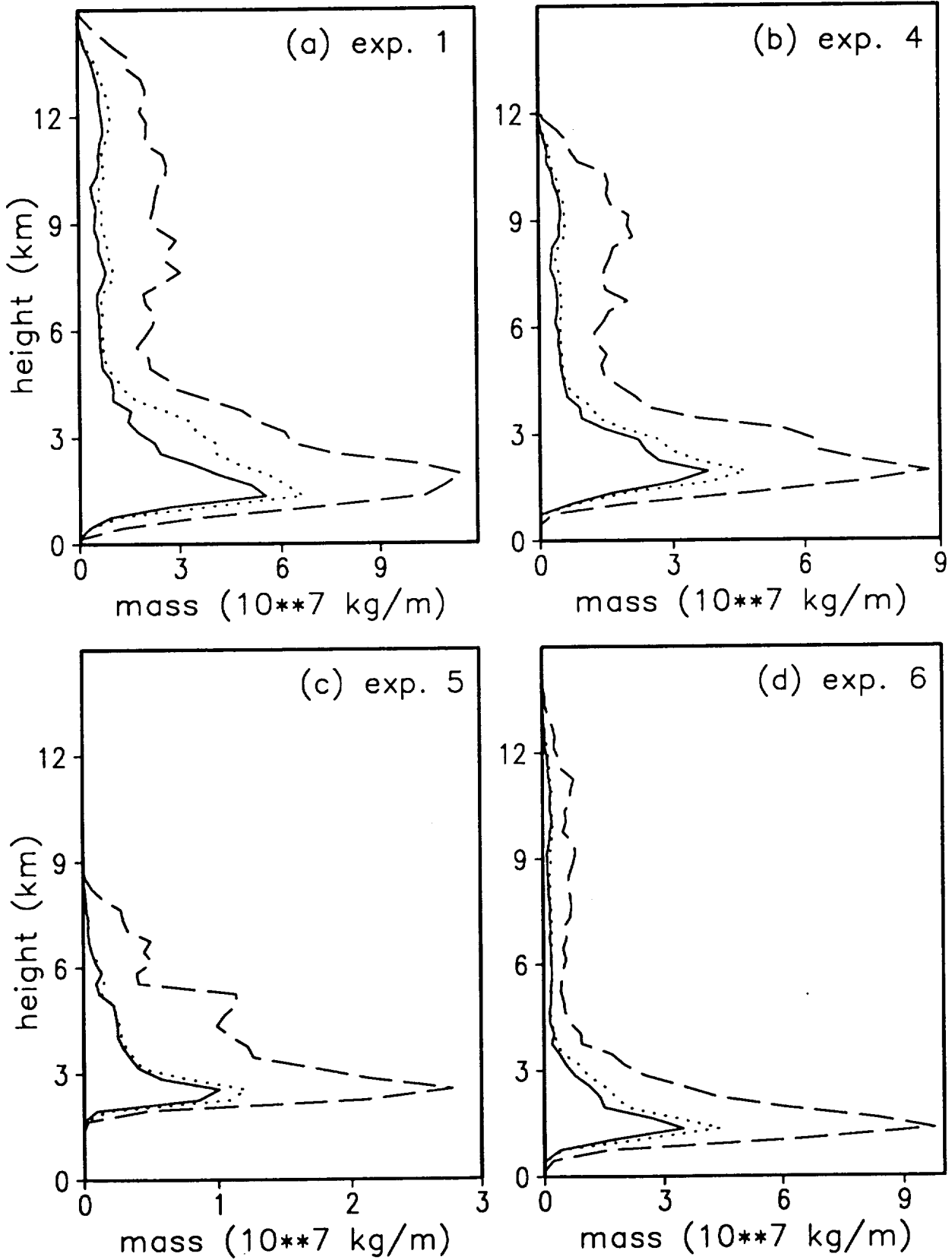


Fig. 11: Mass of environmental air that mixed with updraft air (dashed), mass of environmental air that mixed with updraft air and was entrained into the updraft (solid), and mass of environmental air that was entrained into the updraft, with or without mixing (dotted), for (a) exp. 1, (b) exp. 4, (c) exp. 5, and (d) exp. 6.

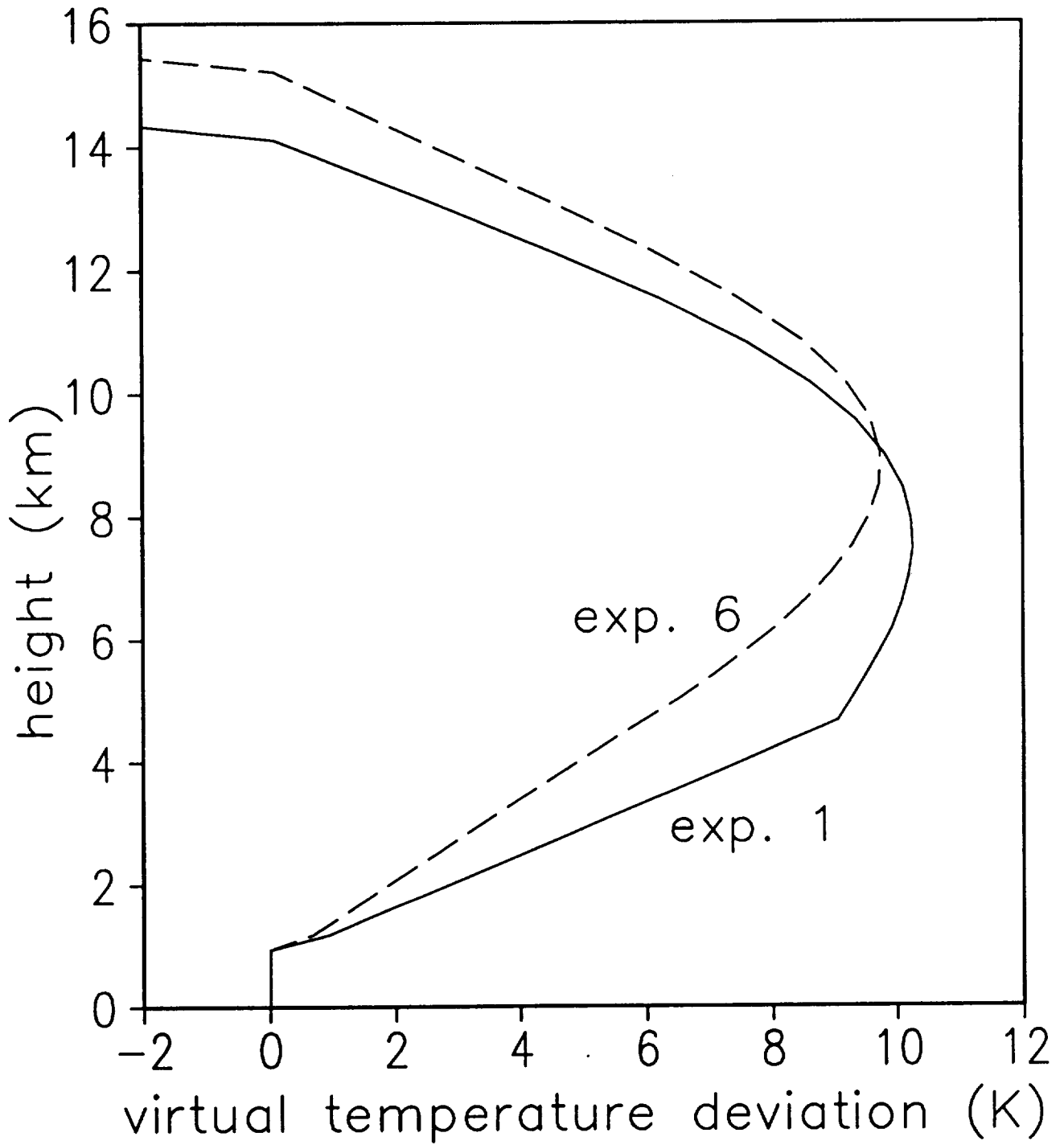


Fig. 12: Virtual temperature of air parcel minus environmental value, for pseudoadiabatic ascent from the surface, using the initial undisturbed soundings of exp. 1 (solid) and exp. 6 (dashed).

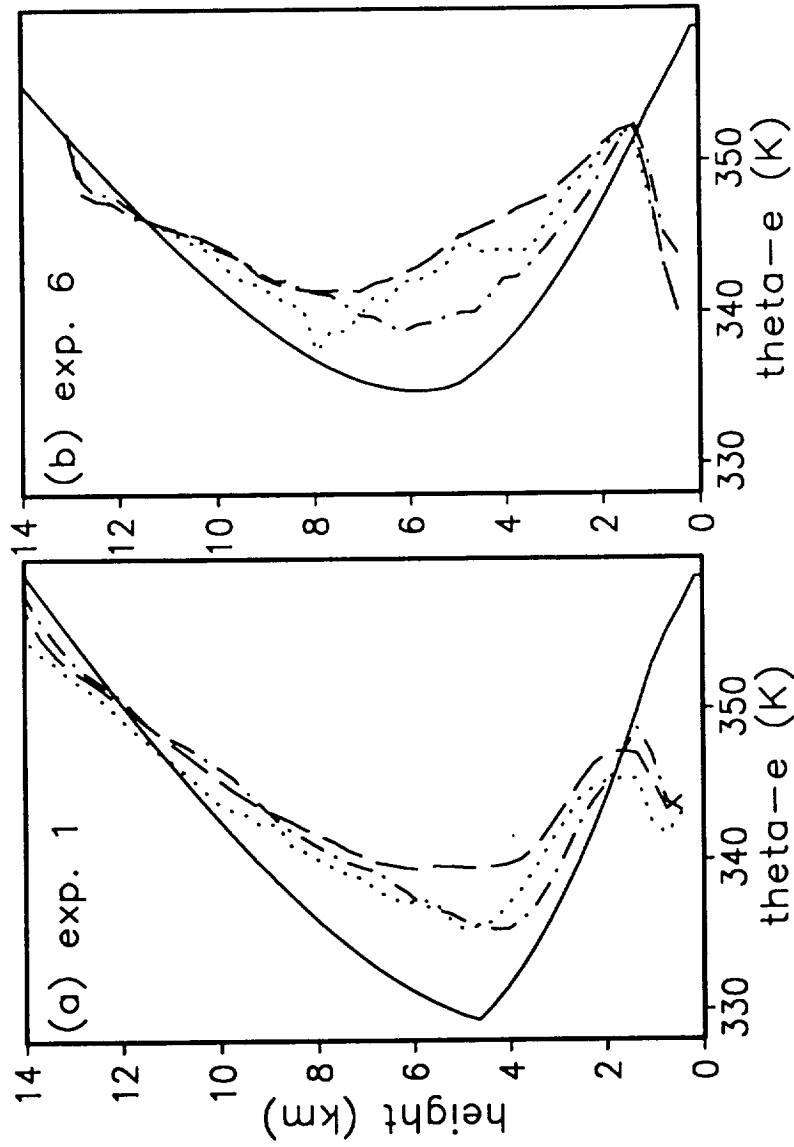


Fig. 13: Equivalent potential temperature in (a) exp. 1 and (b) exp. 6: undisturbed initial sounding (solid), updraft (dashed), entrained by the updraft (dot-dash), and detrained by the updraft (dotted).

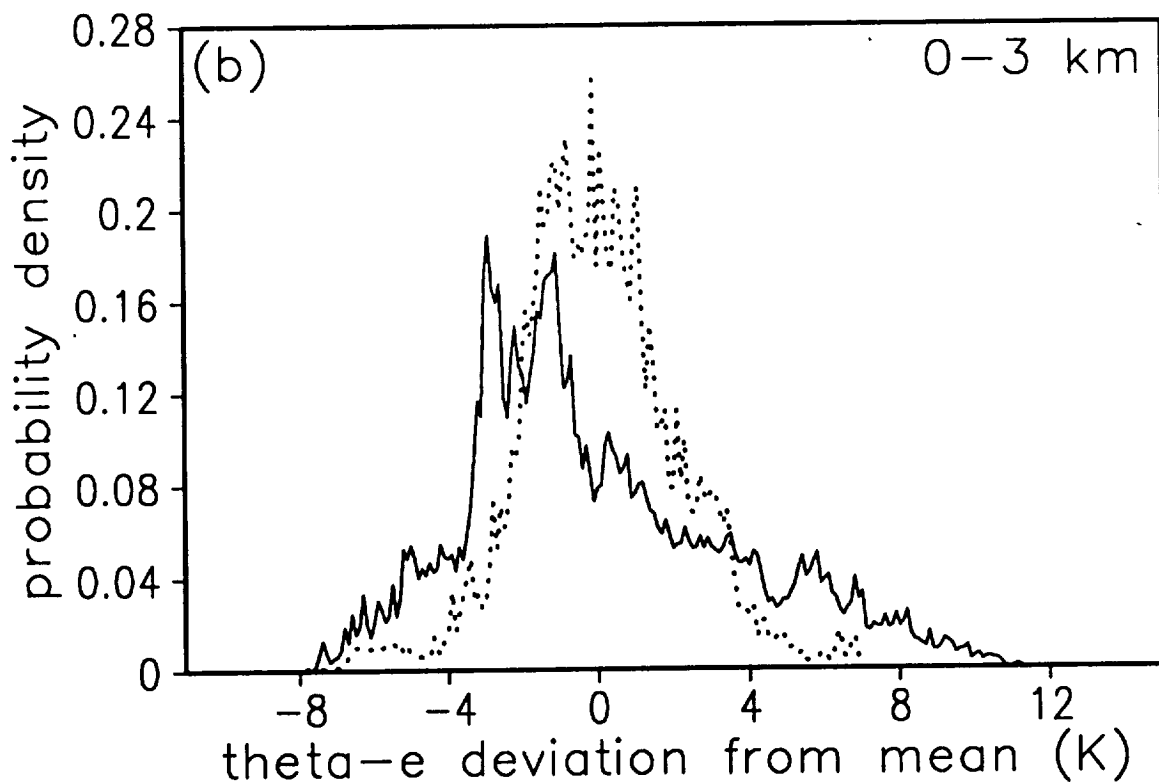
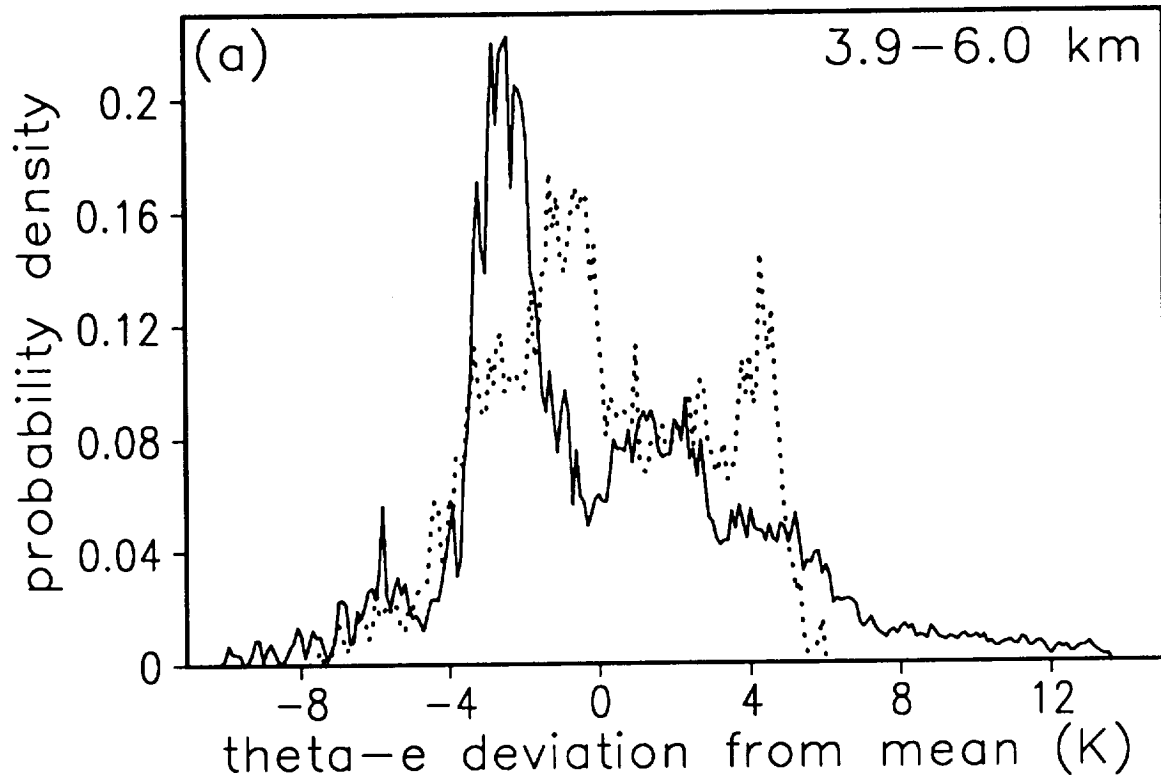


Fig. 14: Probability density function of deviations of updraft equivalent potential temperature from its mean value for updrafts at the same level, for exp. 1 (solid) and exp. 6 (dotted), for (a) the height interval from 3.9 km to 6.0 km, and (b) the height interval from the surface up to 3 km.

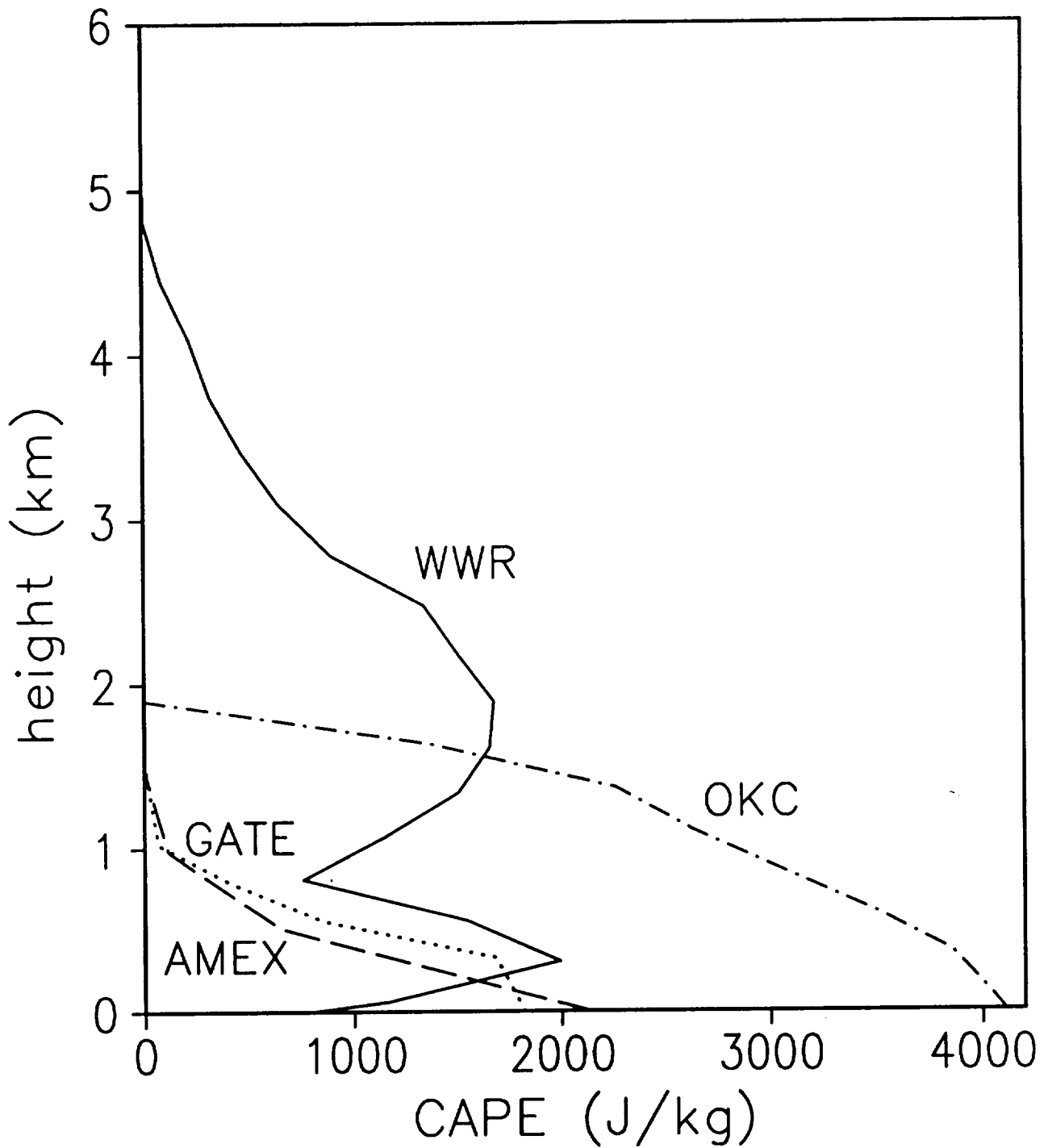


Fig. 15: CAPE computed from soundings observed at Woodward, Oklahoma, 0130 UTC 11 June 1985 (solid), and at Oklahoma City 2030 UTC 10 June 1985 (dot-dash), and for composites of cloud clusters observed during GATE (dotted) and AMEX (dashed). The vertical axis shows the level of origin of the rising parcel.